www.nature.com/npp

American College of Neuropsychopharmacology

ARTICLE

Medial prefrontal cortex input to basolateral amygdala controls acute stress-induced short-term anxiety-like behavior in mice

Wei-Zhu Liu[1,2], Shou-He Huang[2], Yu Wang[1,2], Chun-Yan Wang[1,2], Han-Qing Pan[1,2], Ke Zhao[1,2], Ping Hu[1,3], Bing-Xing Pan[1,2]✉ and Wen-Hua Zhang[1,2,4]✉

Anxiety is a normal and transitory emotional state that allows the organisms to cope well with the real or perceived threats, while excessive or prolonged anxiety is a key characteristic of anxiety disorders. We have recently revealed that prolonged anxiety induced by chronic stress is associated with the circuit-varying dysfunction of basolateral amygdala projection neurons (BLA PNs). However, it is not yet known whether similar mechanisms also emerge for acute stress-induced, short-lasting increase of anxiety. Here, using a mouse model of acute restraint stress (ARS), we found that ARS mice showed increased anxiety-like behavior at 2 h but not 24 h after stress, and this effect was accompanied by a transient increase of the activity of BLA PNs. Specifically, ex vivo patch-clamp recordings revealed that the increased BLA neuronal activity did not differ among the distinct BLA neuronal populations, regardless of their projection targets being the dorsomedial prefrontal cortex (dmPFC) or elsewhere. We further demonstrated that such effects were mainly mediated by the enhanced presynaptic glutamate release in dmPFC-to-BLA synapses but not lateral amygdala-to-BLA ones. Furthermore, while optogenetically weakening the presynaptic glutamate release in dmPFC-to-BLA synapses ameliorated ARS-induced anxiety-like behavior, strengthening the release increased in unstressed mice. Together, these findings suggest that acute stress causes short-lasting increase in anxiety-like behavior by facilitating synaptic transmission from the prefrontal cortex to the amygdala in a circuit-independent fashion.

Neuropsychopharmacology (2023) 48:734–744; https://doi.org/10.1038/s41386-022-01515-x

INTRODUCTION

Anxiety is a transient normal emotional state that drives an adaptive response to potential threats, but if excessive and persistent, it can become pathological and contribute to the development of many psychiatric diseases such as anxiety disorders [1]. Exposure to stressful events is among the most common socioenvironmental factors causing anxiety, with the severity varying with the intensity, duration, and timing of the stressors [2–5]. For example, while acute mild stress can induce short-term anxiety which can soon be recovered, long-term exposure (chronic stress) results in a variety of maladaptive stress responses and triggers anxiety disorders [6–9]. Understanding the neurobiological mechanisms underlying normal and pathological anxiety helps to develop novel effective stress-coping strategies that have major clinical implications for the prevention and treatment of anxiety disorders.

The amygdala has a central role in regulating anxiety responses to stressful and arousing situations [10, 11]. Pharmacological and lesion studies of the amygdala including the basolateral nucleus of the amygdala (BLA) have shown that amygdala activation induces anxiogenic effects, while inactivation results in anxiolytic effects [12, 13]. In the past decade, with the help of state-of-the-art techniques that allow for cellular and circuit-specific manipulations, a burgeoning literature has revealed that BLA projection neurons (PNs) are highly heterogeneous in their connection and function [10, 14]. For example, optogenetic activation of synaptic transmission from the BLA to the ventral hippocampus or dorsomedial prefrontal cortex (dmPFC) produces transient anxiety-like behavior [15, 16]. In addition, studies on animal models of anxiety disorders revealed that both input- and output-specific modulation of BLA neuronal plasticity contributes to the development of chronic stress-induced anxiety disorders. Specifically, chronic stress increases synaptic strength within the dmPFC-amygdala circuit owing to enhanced prefrontal glutamate release onto some, but not the whole population of BLA PNs, particularly onto those projecting to subcortical regions such as the ventral hippocampus [17]. Although the neural circuits in the amygdala underlying prolonged anxiety have begun to be identified [17, 18], whether similar or different mechanisms emerge for short-term anxiety is largely unknown. Considering that anxiety disorders usually develop from frequent and prolonged anxiety, it will be valuable to explore whether and how the distinct neural circuits in the amygdala modulate the occurrence of short-term anxiety under stress conditions. This is also an important addition to understanding anxiety behavior from a physiological and pathological perspective.

To address this issue, we combined in vivo fiber photometry, viral tracing, electrophysiological, optogenetic, and chemogenetic

[1]Department of Biological Science, School of Life Science, Nanchang University, Nanchang 330031, China. [2]Laboratory of Fear and Anxiety Disorders, Institutes of Life Science, Nanchang University, Nanchang 330031, China. [3]Institute of Translational Medicine, Nanchang University, Nanchang 330031 Jiangxi, China. [4]Jiangxi Provincial Key Laboratory of Interdisciplinary Science, Nanchang University, Nanchang 330031, PR China. ✉email: panbingxing@ncu.edu.cn; whzhang@ncu.edu.cn

Received: 4 May 2022 Revised: 25 November 2022 Accepted: 28 November 2022
Published online: 13 December 2022

approaches, to dissect the functional organization of BLA circuits and explore the potential mechanisms in a mouse model of acute restraint stress (ARS). First, we observed that ARS transiently increased the BLA neuronal activity and induced short-term anxiety-like behavior. Next, by dividing the BLA PNs into two subpopulations according to their projection targets (the dmPFC or elsewhere), we found that ARS indistinguishably increased the excitatory synaptic transmission onto both neuronal populations. Notably, ARS selectively increased presynaptic glutamate release from dmPFC inputs but not from lateral amygdala (LA) inputs. Additionally, causal link analysis revealed that the strengthened functional connectivity in the prefrontal cortex-amygdala circuit contributes to acute stress-induced, short-term anxiety-like behavior.

METHODS AND MATERIALS

For detailed methods and materials, see the Supplementary Information.

Animals

All experimental procedures were followed and approved by the Animal Care and Use Committee of Nanchang University (approval No: ncdxsydwll-2018-26). Only male C57BL/6 mice were used for all experiments. Further details can be found in the Supplementary Information.

Acute restraint stress

Eight-week-old male mice were subjected to ARS. The detailed protocol for ARS is provided in the Supplementary Information.

Behavioral test

The elevated plus maze test (EPMT) and open field test (OFT) were performed to monitor anxiety-like behavior as previously described [17, 18]. Detailed methods of the EPMT and OFT are provided in the Supplementary Information.

Stereotaxic surgery

Detailed information on viral and red fluorescent retrograde transported Retrobeads injection is provided in the Supplementary Information.

Fiber photometry

Fiber photometry was performed as previously described [19, 20]. Detailed information was described in the Supplementary Information.

Histology and microscopy

The histology and microscopy methods are described in the Supplementary Information.

Electrophysiological slice recording

The details on electrophysiology can be found in the Supplementary Information.

Chemogenetic and optogenetics

The chemogenetic and optogenetic procedures are described in the Supplementary Information.

Statistical analyses

The statistical analyses were performed using GraphPad Prism 7 (GraphPad Software, Inc., San Diego, CA). All data are shown as the mean ± SEM. p values <0.05 were considered significant. Details on the statistical analyses are available in the Supplementary Information.

RESULTS

ARS transiently increases the neuronal activity of BLA PNs to induce anxiety

Exposure to stressful events always causes anxiety. To explore the effect of acute stress on anxiety-like behavior, we subjected male C57BL/6 mice to 2-h of ARS. Anxiety-like phenotypes in these mice were evaluated 2 and 24 h after ARS (hereafter referred to as ARS-2H and ARS-24H) using the elevated plus maze (EPMT) and OFT. We found that ARS-2H mice displayed a typical anxiogenic phenotype, as indicated by the shorter time spent in and fewer entries into the open arms during the EPMT than control mice (Fig. 1A–D). However, the stressed mice after 24 h of recovery spent a similar time in and had a similar number of entries to the open arms as unstressed control mice (Fig. 1A–D). In line with the EPMT results, in the OFT, ARS-2H but not ARS-24H mice spent a shorter time in the center area of OFT (Fig. 1B, E). The total distance mice traveled in the OFT was comparable in all three groups of mice (Fig. 1F), suggesting that ARS does not affect locomotor activity. These results indicate that ARS induces short-term anxiety-like behavior.

Aberrant BLA activity is highly implicated in the neuropathology of stress-related anxiety [17, 21]; thus, we then explored the impact of ARS on dynamic changes in BLA neural activity using in vivo fiber photometry. To do this, we stereotaxically injected an adeno-associated virus (AAV) expressing GCaMP6s into and implanted optical fiber onto the BLA (Fig. 1G). Four weeks later, we measured the basal level of calcium signals within the BLA. Then the mice were subjected to ARS and the calcium signals were repeatedly measured 2 and 24 h after exposure to ARS. As shown in Fig. 1H, ARS caused dynamic changes in BLA neuronal activity, as indicated by the increased frequency but not the amplitude of calcium signals 2 h after ARS (Post-2H), which then normalized to basal levels by 24 h after ARS (Post-24H) (Fig. 1H–J). However, no obvious changes were observed in control mice (Fig. 1H–J), suggesting that the increased BLA neuronal activity was due to ARS exposure. To further confirm the temporal effects of ARS on BLA neuronal activity, we measured the expression of the immediate early gene c-fos, a marker of neuronal activity. Consistent with the in vivo fiber photometry results, the number of c-fos$^+$ cells in the BLA was significantly increased 2 h after ARS (ARS-2H) compared to that in the control group (Fig. 1K, L). In sharp contrast to measurements made 2 h after ARS, no significant effect was observed 24 h after ARS (ARS-24H) (Fig. 1K, L). These data suggest that ARS triggers transient potentiation of BLA neuronal activity that can be restored 1 day after ARS exposure.

To determine whether the increased activity of BLA PNs was necessary to drive ARS-mediated anxiety-like behavior, we next employed a chemogenetic approach to inactivate BLA PNs and examined its effect on anxiety-like behavior in mice. For this purpose, an AAV expressing hM4Di was bilaterally injected into the BLA, and the efficiency of hM4Di expression was verified by immunohistochemical examination (Fig. 1M, N). To further confirm the effectiveness of chemogenetic inactivation, we directly measured the effect of CNO on the firing of BLA PNs. We observed that the firing rates of BLA PNs were significantly decreased following CNO administration (Fig. 1O). Next, we assessed the anxiety-like behavior of mice when the activity of the BLA PNs was inhibited by CNO administration. As shown in Fig. 1P–S, CNO administration reversed ARS-induced anxiety-like behavior, as indicated by increased open-arm time and open-arm entries of the EPMT (Fig. 1R, S), as well as increased time spent in the center without effects on general locomotor activity (Fig. 1T–V). Then, we studied whether ARS-induced anxiety-like behavior could be blocked by optogenetic silencing of BLA neurons during the ARS session (Supplementary Fig. 1A). We bilaterally injected AAVs expressing eNpHR3.0-mCherry into the BLA and implanted optical fiber into the BLA (Supplementary Fig. 1B, C). Four weeks after viral injection, the mice were subjected to ARS for 2 h, and a single train of light stimulation was delivered during the ARS period (Supplementary Fig. 1A). We found that the optical inhibition of BLA neurons in ARS mice alleviated anxiety-like behavior (Supplementary Fig. 1D–I). These results suggest that the increased BLA neuronal activity contributes to ARS-induced short-term anxiety-like behavior.

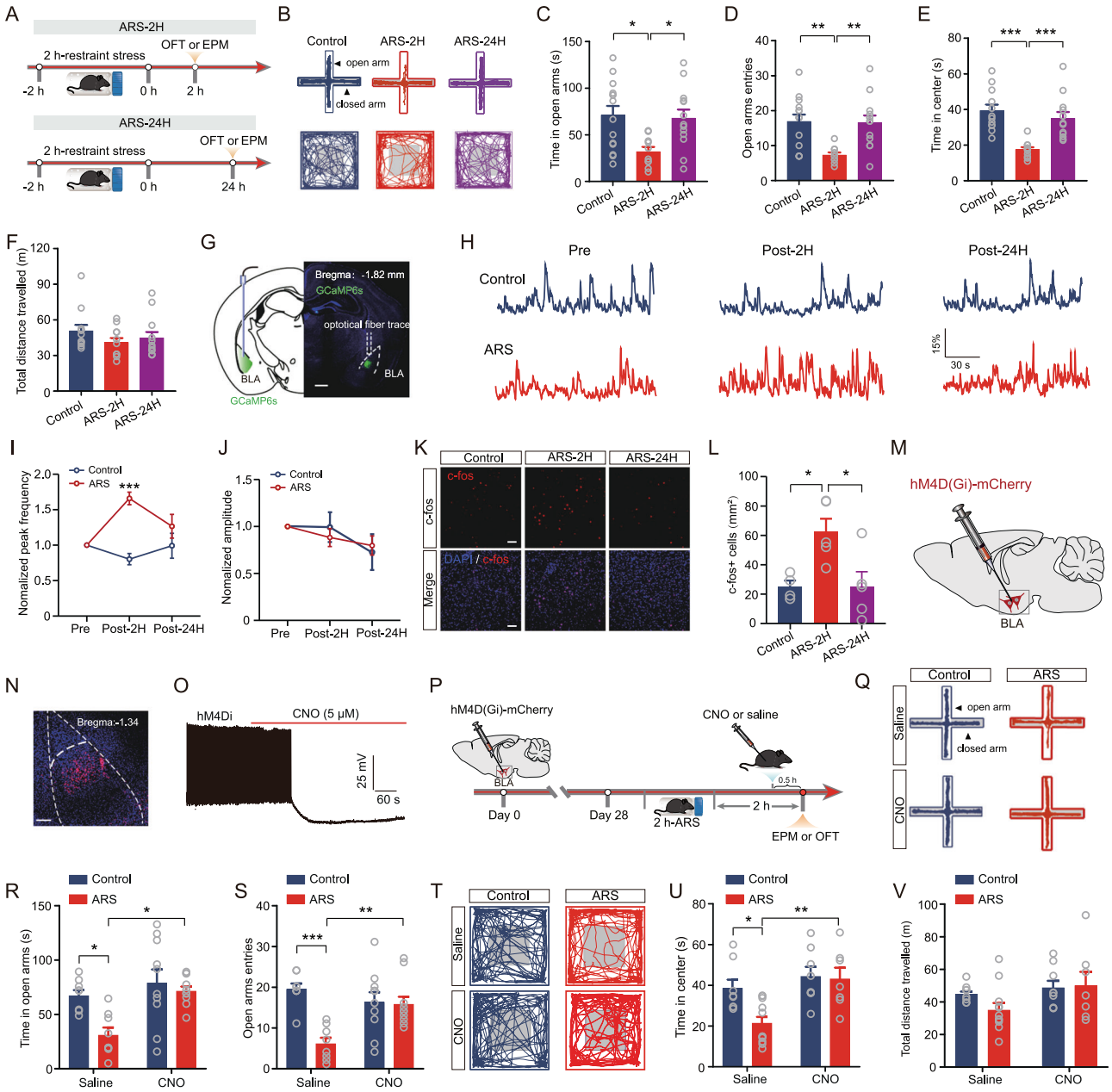

ARS augments the glutamatergic synaptic transmission onto BLA PNs

We next explored the mechanisms underlying the ARS-induced increase in BLA neuronal activity using ex vivo brain slice electrophysiology. Since neuronal activity may be regulated by changes in synaptic plasticity, including excitatory and inhibitory synaptic transmission [22], we first measured the effects of ARS on the excitatory synaptic transmission by recording miniature excitatory postsynaptic currents (mEPSCs) from acutely isolated ex vivo slices (Fig. 2A). Compared to unstressed control mice, ARS-2H mice exhibited a dramatically increased mean frequency of mEPSCs and a left-shifted cumulative probability distribution of inter-mEPSC intervals in BLA PNs, while such changes were normalized 24 h after ARS (Fig. 2B–D). However, the mean amplitude and the cumulative probability distributions of mEPSCs amplitude were comparable among the three groups of mice (Fig. 2E, F). We next tested the possible effects of ARS on GABAergic inhibitory transmission onto BLA PNs by recording the miniature inhibitory postsynaptic currents (mIPSCs). However, unlike excitatory transmission onto BLA PNs, both the frequency and amplitude of mIPSCs remained unaltered in all three groups of mice (Fig. 2G–K).

In addition to synaptic plasticity, neurons also exhibit a form of nonsynaptic plasticity that enables them to modify intrinsic excitability in response to external activity [20, 23, 24]. Thus, we examined the potential influence of ARS on the intrinsic excitability of BLA PNs. By injecting a depolarizing current pulse with a step increase of 50 pA into the recorded cells to evoke action potentials (APs), we found that ARS had no significant effect on the changes in AP numbers (Fig. 2L, M). We also measured the intrinsic excitability of BLA PNs by injecting ramped depolarization currents. In line with the above results, neither ARS-2H nor ARS-24H impacted the neuronal firing or rheobase (Supplementary Fig. 2). We then explored whether these ARS-induced electrophysiological changes could be blocked by optogenetic silencing of BLA neurons during the ARS session. Interestingly, inhibiting BLA neurons blocked the ARS-induced increase in the frequency of mEPSCs (Supplementary Fig. 3).

Fig. 1 Acute stress transiently increases the neuronal activity of BLA projection neurons and anxiety-like behavior. A Experimental procedures. **B** Representative activity tracking in EPMT (upper) and OFT. Summary plots of time in open arms (**C**) and open-arm entries (**D**) during EPMT. Control mice: $n = 14$ mice; ARS-2H mice, $n = 10$ mice; ARS-24H mice, $n = 13$ mice. Time in open arms: one-way ANOVA measures, $F_{(2,34)} = 5.332$, $p = 0.0097$. Bonferroni post hoc comparison, ARS-2H vs. control, $^{*}p < 0.05$; ARS-2H vs. ARS-24H, $^{*}p < 0.01$. Open-arm entries: one-way ANOVA measures, $F_{(2,34)} = 8.214$, $p = 0.0012$. Bonferroni post hoc comparison, ARS-2H vs. control, $^{**}p < 0.01$; ARS-2H vs. ARS-24H, $^{**}p < 0.01$. Summary plots of time in center area (**E**) and total distance traveled (**F**) during OFT. Control mice: $n = 12$ mice; ARS-2H mice, $n = 11$ mice; ARS-24H mice, $n = 12$ mice. Time in center: one-way ANOVA measures, $F_{(2,32)} = 14.31$, $p < 0.0001$. Bonferroni post hoc comparison, ARS-2H vs. control, $^{***}p < 0.001$; ARS-2H vs. ARS-24H, $^{***}p < 0.01$. Total distance traveled: one-way ANOVA measures, $F_{(2,32)} = 1.11$, $p = 0.3418$. **G** Representative image showing GCaMP6s expression and the cannula implantation onto BLA. Scale bar: 500 μm. **H** Representative traces of filtered calcium signals in Control (upper) and ARS (lower) mice. **I** Summary plots of normalized peak frequency as a function of pre, 2 h post, and 24 h post ARS. Data were normalized to pre-ARS periods for all mice. Control mice: $n = 6$ mice; ARS mice, $n = 7$ mice. Two-way ANOVA with repeated measures, main effect of stress treatment, $F_{(1,11)} = 10.44$, $p = 0.008$; main effect of time, $F_{(2,22)} = 3.244$, $p = 0.058$; interaction, $F_{(2,22)} = 11.56$, $p = 0.0004$. Bonferroni post hoc comparison, ARS vs. control, $^{***}p < 0.001$. **J** Same as in **E** except that the data were from normalized peak amplitude. Two-way ANOVA with repeated measures, main effect of stress treatment, $F_{(1,11)} = 0.0162$, $p = 0.901$; main effect of time, $F_{(2,22)} = 2.971$, $p = 0.0721$; interaction, $F_{(2,22)} = 0.405$, $p = 0.672$. **K** Representative images showing c-fos expression in BLA for control (Control), 2 h post ARS (ARS-2H) and 24 h post ARS (ARS-24H) mice. Scale bar = 100 μm. **L** Summary plots of c-fos^{+} cells expression in BLA. Control mice: $n = 4$ mice; ARS-2H mice, $n = 5$ mice; ARS-24H mice, $n = 5$ mice. One-way ANOVA with repeated measures, $F_{(2,11)} = 6.244$, $p = 0.0154$. Bonferroni post hoc comparison, ARS-2H vs. control, $^{*}p < 0.05$; ARS-2H vs. ARS-24H, $^{*}p < 0.05$. **M** Diagram showing the injection of hM4D(Gi)-carrying adeno-associated virus (AAV) vectors into the BLA. **N** Representative image showing hM4D(Gi) expression in BLA. Scale bar = 100 μm. **O** Representative trace showing CNO-induced inhibition of firing of BLA projection neuron. **P** Experimental procedures. **Q** Representative activity tracking during EPMT. Summary plots of time in open arms (**R**) and open-arm entries (**S**) during EPMT. Saline: control mice: $n = 8$ mice; ARS mice, $n = 8$ mice; CNO: control mice, $n = 10$ mice; ARS mice, $n = 10$ mice. Time in open arms: two-way ANOVA with repeated measures, main effect of virus treatment, $F_{(1,32)} = 6.743$, $p = 0.0141$; main effect of stress, $F_{(1,32)} = 9.551$, $p = 0.0041$; interaction, $F_{(1,32)} = 2.95$, $p = 0.0955$, Bonferroni post hoc analysis, Saline: control mice vs. ARS mice, $^{*}p < 0.05$. Open-arm entries: two-way ANOVA with repeated measures, main effect of virus treatment, $F_{(1,32)} = 12.3$, $p = 0.0014$; main effect of stress, $F_{(1,32)} = 2.68$, $p = 0.1114$; interaction, $F_{(1,32)} = 10.6$, $p = 0.0027$, Bonferroni post hoc analysis, Saline: control mice vs. ARS mice, $^{***}p < 0.001$. **T** Representative activity tracking during OFT. Summary plots of time in center area (**U**) and total distance traveled (**V**) during OFT. Saline: control mice: $n = 8$ mice; ARS mice, $n = 11$ mice; CNO: control mice, $n = 8$ mice; ARS mice, $n = 7$ mice. Time in center: two-way ANOVA with repeated measures, main effect of virus treatment, $F_{(1,30)} = 4.513$, $p = 0.0042$; main effect of stress, $F_{(1,30)} = 10.18$, $p = 0.0033$; interaction, $F_{(1,30)} = 3.37$, $p = 0.0763$, Bonferroni post hoc analysis, Saline: control mice vs. ARS mice, $^{*}p < 0.05$. Total distance traveled: two-way ANOVA with repeated measures, main effect of virus treatment, $F_{(1,30)} = 0.6634$, $p = 0.4218$; main effect of stress, $F_{(1,30)} = 3.539$, $p = 0.0697$; interaction, $F_{(1,30)} = 1.112$, $p = 0.3$. All data are presented as the mean ± SEM.

Altogether, these findings strongly suggest that ARS transiently increases BLA neuronal activity by transiently increasing glutamatergic transmission, which is different from the effects of chronic stress since both glutamatergic transmission and intrinsic excitability contribute to chronic stress-induced hyperactivation of BLA PNs [18, 25].

ARS indistinguishably enhances the efficacy of synaptic transmission onto distinct populations of BLA PNs

Mounting evidence suggests that BLA PNs are highly heterogeneous regarding their downstream projection targets and functions [26, 27]. We then explored whether ARS differentially impacts different populations of BLA PNs. Considering that the BLA-dmPFC circuits play a critical role in mediating the stress response, we divided BLA PNs into two subpopulations: those that projected to the dmPFC (BLA → dmPFC PNs) and those that projected elsewhere (BLA ↛ dmPFC PNs). To do this, we injected red fluorescent retrobeads into the dmPFC to identify the two populations; the former were beads-labeled neurons and the unlabeled putatively belonged to the latter subpopulation (Fig. 3A–C). The effects of ARS on mEPSCs, were then explored in the two clusters of BLA PNs. In BLA → dmPFC PNs, ARS-2H markedly increased the mEPSCs frequency but not amplitude, an effect that was reversed 24 h after ARS (Fig. 3D–F). Moreover, ARS-2H considerably left-shifted the cumulative probability of the mEPSCs interval, whereas it right-shifted the cumulative probability of the mEPSCs amplitude; these values were normalized 24 h post-stress (Fig. 3G, H). Surprisingly, in striking contrast to the differential regulation of synaptic plasticity by chronic stress [25, 28], similar effects were observed in BLA ↛ dmPFC PNs (Fig. 3I–M). However, no changes in the mIPSCs and APs in BLA PNs were found in either population after ARS (Supplementary Figs. 4 and 5). Collectively, these data suggest that ARS indistinguishably alters the efficacy of synaptic transmission onto both BLA → dmPFC and BLA ↛ dmPFC PNs.

ARS selectively increases glutamate release in the dmPFC-BLA pathway

The efficacy of synaptic transmission can be altered by mechanisms of presynaptic neurotransmitter release and/or postsynaptic receptor-mediated event. We first measured the effect of ARS on the probability of glutamate release by recording paired-pulse ratio (PPR), which is inversely correlated with the probability of presynaptic neurotransmitter release (Pr), in the BLA → dmPFC and BLA ↛ dmPFC PNs. Then, as the lateral nucleus of the amygdala (LA) is known as the input station of the amygdala by receiving and integrating multiple sensory afferents to the BLA, we placed a bipolar stimulation electrode in the LA, and recorded the evoked EPSCs on two consecutive electrical stimuli (separated by 100 ms) in the BLA (Fig. 4A). Somewhat surprisingly, ARS did not alter the efficacy of PPR in either population (Fig. 4B, C).

The BLA also receives dense inputs from the dmPFC, and the highly reciprocal connection between the dmPFC and BLA has been shown to play an essential role in regulating emotion-related behaviors [29–31]. Thus, we then examined the PPR within the dmPFC-BLA circuit using optogenetic techniques. For this, we co-injected AAV expressing ChR2 and red fluorescent retrobeads into the dmPFC (Fig. 4D). Consistent with previous finding [32], ChR2-expressing dmPFC fibers were observed mainly in the BLA (Fig. 4D). By delivering two consecutive light pulses (separated by 100 ms) to excite the dmPFC afferents, we recorded PPR in the BLA → dmPFC and BLA ↛ dmPFC PNs (Fig. 4E, F). Interestingly, the PPR in the two clusters was lower in ARS-2H mice than in unstressed control mice; the value was normalized to baseline in ARS-24H mice (Fig. 4G, H).

Taken together, these results suggest that ARS selectively increases Pr in the dmPFC but not LA inputs to the two populations in the BLA.

ARS does not affect postsynaptic plasticity within dmPFC-BLA synapses

Following the observation that ARS temporally increased the presynaptic release probability within the dmPFC-BLA circuit, we

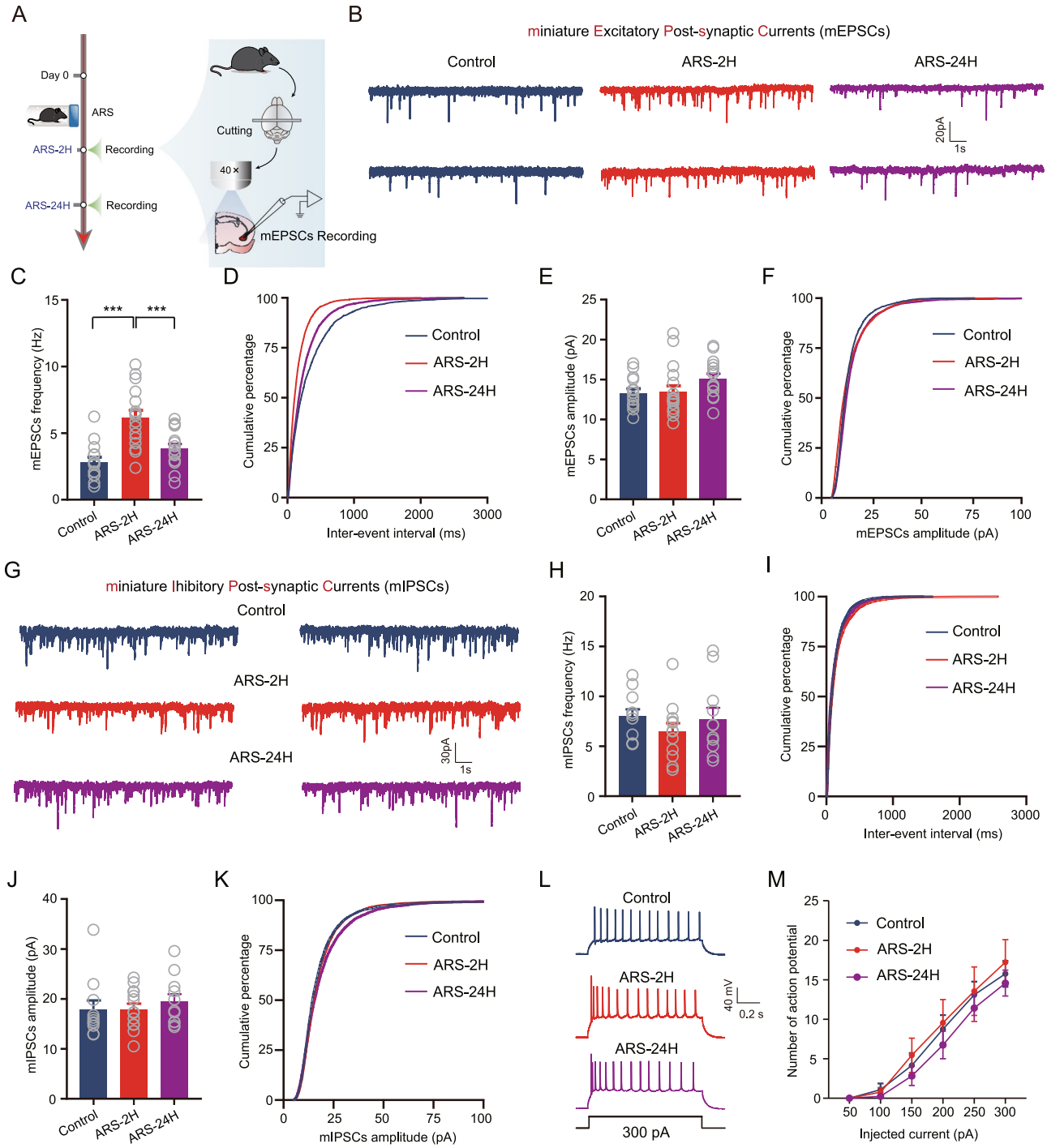

Fig. 2 ARS augments the glutamatergic synaptic transmission onto BLA PNs. A Experimental procedures for electrophysiology recording experiments. **B** Representative traces showing miniature excitatory postsynaptic currents (mEPSCs) (scale bar: 1 s, 20 pA). Summary plots of averaged mEPSC frequency (**C**) and cumulative probability of the interevent interval (**D**). Control mice: $n = 15$ neurons/5 mice; ARS-2H mice, $n = 17$ neurons/6 mice; ARS-24H mice, $n = 16$ neurons/5 mice. Frequency: one-way ANOVA measures, $F_{(2,45)} = 16.45$, $p < 0.0001$. Bonferroni post hoc comparison, ARS-2H vs. control, ***$p < 0.001$; ARS-2H vs. ARS-24H, ***$p < 0.001$. Summary plots of averaged mEPSC amplitude (**E**) and cumulative probability of the amplitude (**F**). Control mice: $n = 15$ neurons/5 mice; ARS-2H mice, $n = 17$ neurons/6 mice; ARS-24H mice, $n = 16$ neurons/5 mice. Amplitude: one-way ANOVA measures, $F_{(2,45)} = 2.495$, $p = 0.939$. **G** Representative traces showing miniature inhibitory postsynaptic currents (mIPSCs) (scale bar = 1 s, 30 pA). Summary plots of averaged mIPSCs frequency (**H**) and cumulative probability of the interevent interval (**I**). Control mice: $n = 11$ neurons/3 mice; ARS-2H mice, $n = 12$ neurons/4 mice; ARS-24H mice, $n = 11$ neurons/3 mice. Frequency: one-way ANOVA measures, $F_{(2,31)} = 0.815$, $p = 0.4519$. Summary plots of averaged mIPSCs amplitude (**J**) and cumulative probability of the amplitude (**K**). Control mice: $n = 11$ neurons/3 mice; ARS-2H mice, $n = 12$ neurons/4 mice; ARS-24H mice, $n = 11$ neurons/3 mice. Amplitude: Kruskal–Wallis H test, Kruskal–Wallis statistic: 1.439, $p = 0.4871$. **L** Representative traces showing the firing in response to 300 pA injected current. **M** Summary plots of action potentials (APs) number as a function of the injected current strength. Control mice: $n = 12$ neurons/4 mice; ARS-2H mice, $n = 9$ neurons/3 mice; ARS-24H mice, $n = 12$ neurons/4 mice. Two-way ANOVA with repeated measures, main effect of stress treatment, $F_{(2,30)} = 0.4472$, $p = 0.6436$; main effect of time, $F_{(5,150)} = 128.6$, $p < 0.0001$; interaction, $F_{(10,150)} = 0.4054$, $p = 0.9424$. All data are presented as the mean ± SEM.

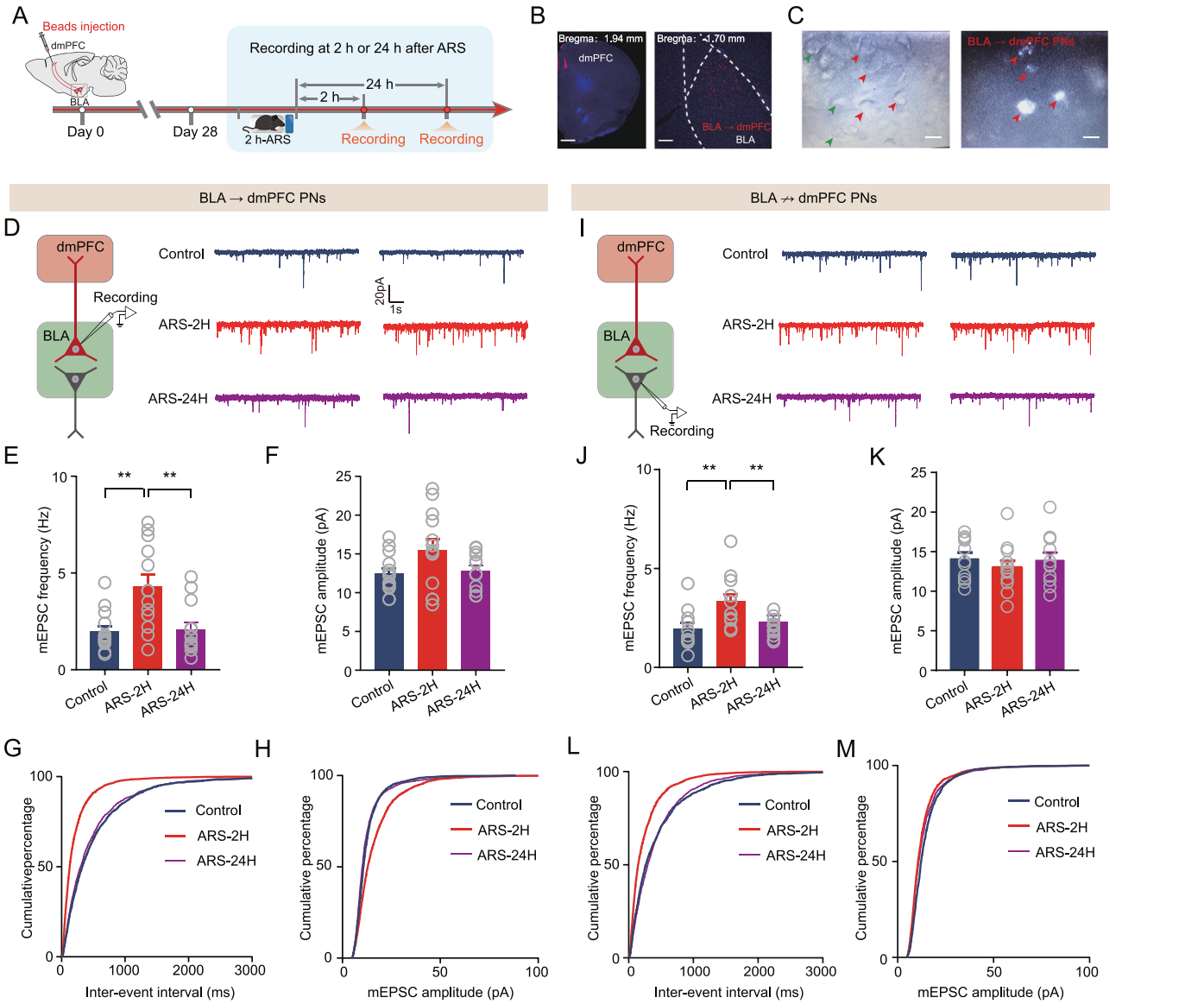

Fig. 3 Acute stress enhances glutamatergic transmission onto onto both BLA → dmPFC and BLA ↛ dmPFC PNs. A Schematic showing the experimental procedures. **B** Representative images showing the injection site in dmPFC (left) and red Retrobeads-labeled BLA → dmPFC PNs (right). Scale bar: 500 (left) and 100 (right) μm. **C** Infrared DIC (left) or fluorescent (right) images of BLA → dmPFC (red arrow heads) or BLA ↛ dmPFC PNs (green arrow heads). scale bar: 10 μm. **D** Representative traces showing mEPSCs in BLA → dmPFC PNs (scale bar:1 s, 20 pA). Summary plots of averaged mEPSC frequency (**E**) and averaged mEPSC amplitude (**F**) in BLA → dmPFC PNs. Control mice: $n = 14$ neurons/5 mice; ARS-2H mice, $n = 13$ neurons/4 mice; ARS-24H mice, $n = 13$ neurons/4 mice. Frequency: Kruskal–Wallis *H* test, Kruskal–Wallis statistic: 11.03, $p = 0.004$. Dunn's post hoc comparison, ARS-2H vs. control, $^{**}p < 0.01$; ARS-24H vs. ARS-2H, $^{**}p < 0.01$. Amplitude: one-way ANOVA measures, $F_{(2,37)} = 3.08$, $p = 0.0579$. Summary plots of cumulative probability of the interevent interval (**G**) and cumulative probability of the amplitude (**H**) of mEPSCs in BLA → dmPFC PNs. **I** Representative traces showing mEPSCs in BLA ↛ dmPFC PNs (scale bar:1 s, 20 pA). Summary plots of average mEPSC frequency (**J**) and averaged mEPSC amplitude (**K**) in BLA ↛ dmPFC PNs. Control mice: $n = 11$ neurons/4 mice; ARS-2H mice, $n = 12$ neurons/4 mice; ARS-24H mice, $n = 11$ neurons/4 mice. Frequency: one-way ANOVA measures, $F_{(2,31)} = 7.06$, $p = 0.003$. Bonferroni post hoc comparison, ARS-2H vs. control, $^{**}p < 0.01$; ARS-24H vs. ARS-2H, $^{**}p < 0.01$. Amplitude: one-way ANOVA measures, $F_{(2,31)} = 0.4728$, $p = 0.6277$. **L**, **M** Summary plots of cumulative probability of the interevent interval (**L**) and cumulative probability of the amplitude (**M**) of mEPSCs in BLA ↛ dmPFC PNs. All data are presented as the mean ± SEM.

explored whether ARS also affects postsynaptic plasticity within the dmPFC-BLA pathway. Two approaches were used in this study. First, we examined the ratio of dmPFC-driven, AMPA receptor-mediated EPSCs to those mediated by NMDA receptors in the two populations (AMPA/NMDA ratio), which measures postsynaptic changes in synaptic strength. We found that ARS did not affect the ratio in either population (Supplementary Fig. 6A–D). Second, we recorded asynchronous quantal responses induced by stimulating dmPFC afferents in the presence of equal concentrations of strontium ions (Sr^{2+}), substituted for extracellular Ca^{2+}. Consistent with the increased presynaptic glutamate levels in both populations of BLA PNs, ARS-2H elevated the frequency of the quantal response in the synapses in both subsets of BLA PNs. In contrast, the quantal size of the asynchronous quantal response was not altered by ARS (Supplementary Fig. 6E–J). In addition, we also compared the LA-driven AMPA/NMDA ratio in the two populations. Similarly, no significant stress-induced changes were observed (Supplementary Fig. 7). These results suggest that ARS does not affect the postsynaptic function of dmPFC-BLA synapses.

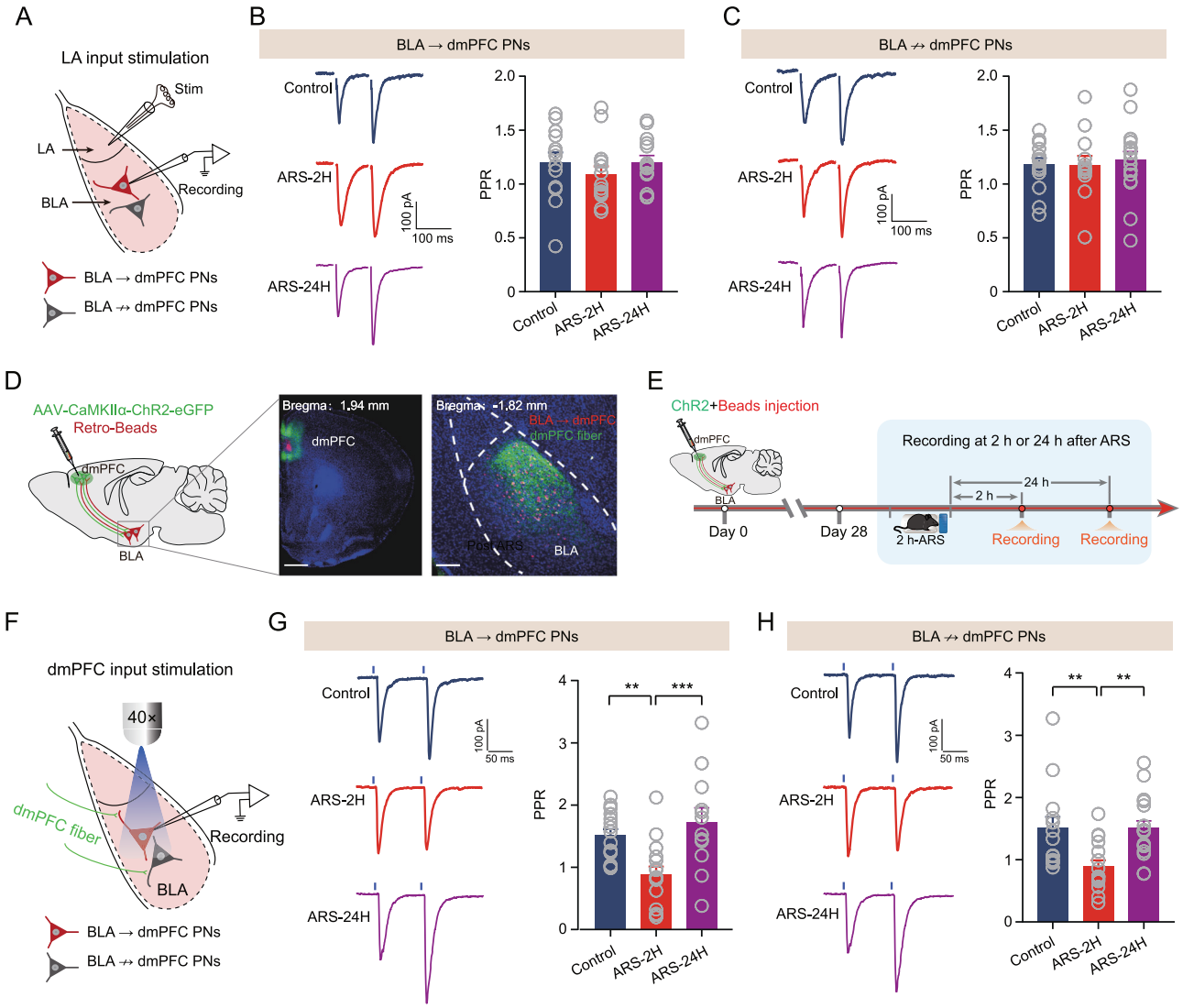

Fig. 4 Acute stress selectively augments dmPFC-evoked glutamatergic transmission onto BLA PNs. A Schematic showing recording of BLA → dmPFC or BLA ↛ dmPFC PNs in response to electrostimulation of LA inputs. **B** Representative traces showing evoked EPSCs in BLA → dmPFC PNs upon paired electrostimulation of LA inputs (separated by 100 ms). Scale bar: 100 ms, 100 pA (left) and summary plots of paired pulse ratio (PPR) in dmPFC → BLA PNs (right). Control mice: $n = 13$ neurons/4 mice; ARS-2H mice, $n = 15$ neurons/5 mice; ARS-24H mice, $n = 14$ neurons/4 mice. One-way ANOVA measures, $F_{(2,39)} = 0.6918$, $p = 0.5067$. **C** Same as in **B** except that the data were from BLA ↛ dmPFC PNs. Control mice: $n = 15$ neurons/5 mice; ARS-2H mice, $n = 13$ neurons/4 mice; ARS-24H mice, $n = 18$ neurons/6 mice. One-way ANOVA measures, $F_{(2,43)} = 0.1332$, $p = 0.8757$. **D** Schematic showing co-injection of ChR2-carrying AAV and red fluorescent Retrobeads into dmPFC. Retrobeads were used to differentiate the putative BLA → dmPFC and BLA ↛ dmPFC PNs in BLA (left) and representative images showing the injection site in dmPFC (middle) and red Retrobeads-labeled BLA → dmPFC PNs and dmPFC inputs in BLA (right). Scale bar: 500 (middle) and 100 (right) μm. **E** Schematic showing the experimental procedures. **F** Schematic showing recording of the postsynaptic responses in BLA → dmPFC or BLA ↛ dmPFC PNs to optogenetic activation of dmPFC inputs. **G** Representative traces showing evoked EPSCs in BLA → dmPFC upon paired light stimuli of dmPFC inputs (separated by 100 ms). Scale bar: 50 ms, 100 pA (left) and summary plots of paired pulse ratio (PPR) in BLA → dmPFC PNs (right). Control mice: $n = 17$ neurons/6 mice; ARS-2H mice, $n = 16$ neurons/5 mice; ARS-24H mice, $n = 12$ neurons/4 mice. One-way ANOVA measures, $F_{(2,42)} = 8.986$, $p = 0.0006$. Bonferroni post hoc comparison, ARS-2H vs. control, $^{**}p < 0.01$; ARS-24H vs. ARS-2H, $^{***}p < 0.001$. **H** Same as in **G** except that the data were from BLA ↛ dmPFC PNs. Control mice: $n = 15$ neurons/5 mice; ARS-2H mice, $n = 16$ neurons/5 mice; ARS-24H mice, $n = 17$ neurons/6 mice. Kruskal–Wallis *H* test, Kruskal–Wallis statistic: 14.36, $p < 0.001$. Dunn's post hoc comparison, ARS-2H vs. control, $^{**}p < 0.01$; ARS-24H vs. ARS-2H, $^{***}p < 0.001$. All data are presented as the mean ± SEM.

Optogenetic inhibition of prefrontal glutamate release alleviates anxiety-like behavior in ARS mice

Since the dmPFC inputs to BLA were potentiated by ARS-2H and the altered pattern was highly consistent with the time window of ARS-induced anxiety-like behavior, we then asked whether reducing prefrontal glutamate release within the dmPFC-to-BLA synapse would alleviate ARS-induced anxiety-like behavior. To do this, mice injected with ChR2-eGFP were subjected to ARS and, 2 h after stress, a single train of low-frequency light stimulation (LFS), which was shown to efficiently decrease the Pr within dmPFC-to-BLA synapses in our previous study [17], was delivered to ARS mice (Fig. 5A–C). We first examined the effect of LFS on mEPSCs frequency in both neuronal populations in ARS mice. LFS markedly reduced mEPSC frequency without any effect on amplitude in both neuronal populations in ARS mice (Supplementary Fig. 8). We then measured anxiety-like behavior after LFS. As shown in Fig. 5D, E, after LFS treatment, the mice spent more time in the center region but did not alter the total distance traveled during OFT. In

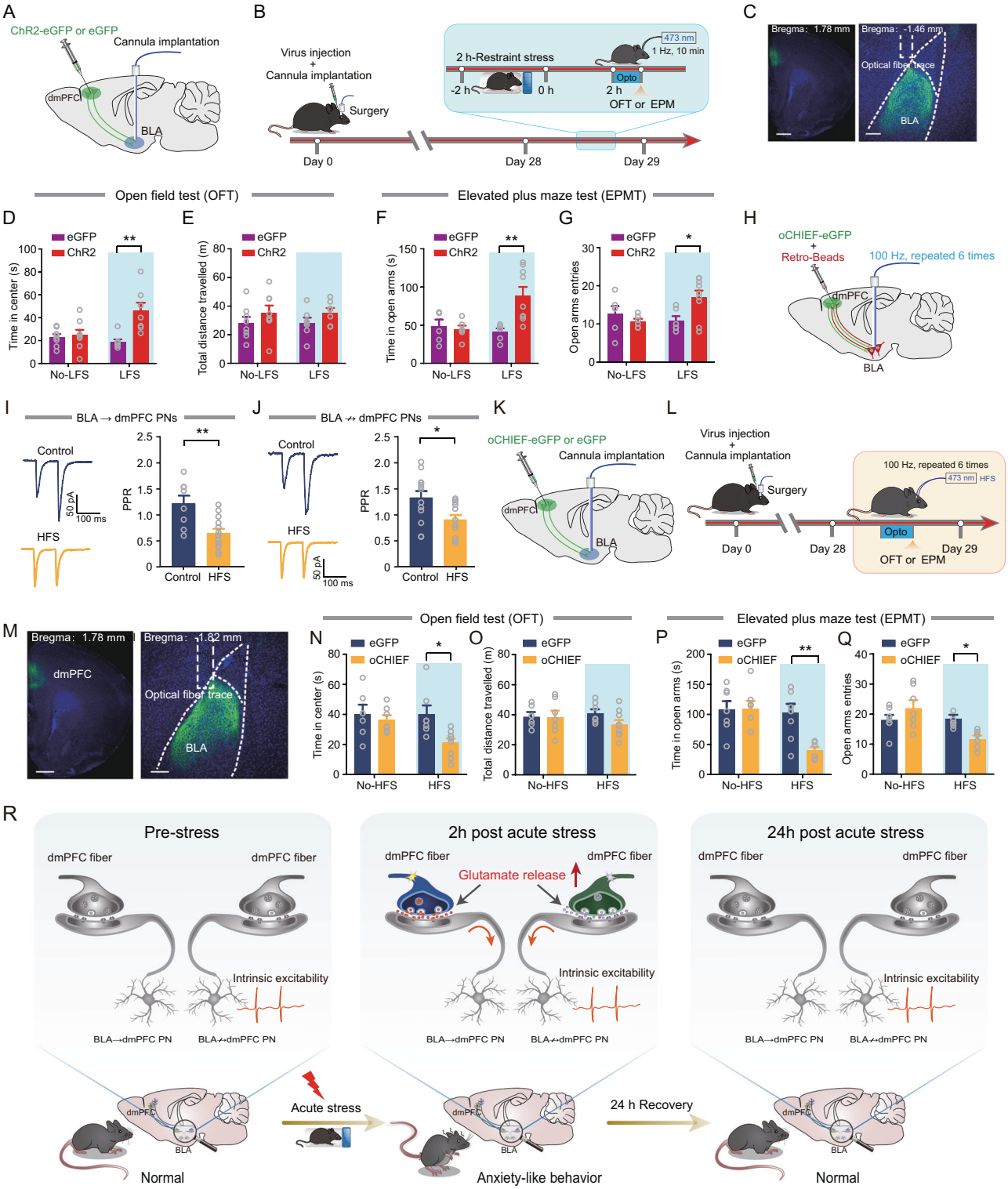

the EPMT, the LFS-treated mice spent more time in and had more entries to the open arms (Fig. 5F, G). However, in eGFP-expressing mice, the LFS failed to affect these behavioral parameters (Fig. 5D–G). In addition, optogenetic inhibition of dmPFC-to-BLA circuit during the ARS session also mitigated ARS-induced anxiety-like behavior (Supplementary Fig. 9). These results suggest that decreasing prefrontal glutamate release within the dmPFC-to-BLA synapses alleviates ARS-induced anxiety-like behavior.

Optogenetic augmentation of prefrontal glutamate release increases anxiety-like behavior in unstressed mice

Last, to explore whether increased prefrontal glutamate release onto BLA PNs is sufficient to mimic the influence of ARS on mice's anxiety-like behavior, we first attempted to find an approach to enhance the Pr in dmPFC inputs to the BLA PNs in unstressed mice. The high-frequency light stimulation (HFS) protocol was previously shown to successfully enhance glutamatergic transmission and alter mouse behavior in a previous study [33]. Therefore,

Fig. 5 Optogenetic inhibition or augmentation of prefrontal glutamate release modulates anxiety-like behavior. A Schematic illustration of injection of ChR2- or eGFP-carrying AAV in dmPFC. **B** Schematic showing the experimental procedures. **C** Representative images showing the injection site in dmPFC (left) and optic fibers placement onto BLA (right). Scale bar: 500 (left) and 100 (right) μm. OFT time in center (**D**) and total distance (**E**) measured LFS a. No-LFS: eGFP mice: $n = 8$ mice; ChR2 mice, $n = 8$ mice; LFS: eGFP mice, $n = 7$ mice; ChR2 mice, $n = 7$ mice. Time in center: two-way ANOVA with repeated measures, main effect of LFS treatment, $F_{(1,26)} = 10.34$, $p = 0.0035$; main effect of virus, $F_{(1,26)} = 3.414$, $p = 0.076$; interaction, $F_{(1,26)} = 7.869$, $p = 0.0094$, Bonferroni post hoc analysis, LFS: eGFP mice vs. ChR2 mice, $^{**}p < 0.001$. Total distance traveled: two-way ANOVA with repeated measures, main effect of LFS treatment, $F_{(1,26)} = 3.003$, $p = 0.0949$; main effect of virus, $F_{(1,26)} = 0.0006$, $p = 0.9808$; interaction, $F_{(1,26)} = 0.0022$, $p = 0.963$. EPM open-arm time (**F**) and entries (**G**) measured LFS. No-LFS: eGFP mice: $n = 6$ mice; ChR2 mice, $n = 6$ mice; LFS: eGFP mice, $n = 6$ mice; ChR2 mice, $n = 9$ mice. Time in open arms: two-way ANOVA with repeated measures, main effect of LFS treatment, $F_{(1,23)} = 5.406$, $p = 0.0292$; main effect of virus, $F_{(1,23)} = 3.991$, $p = 0.0577$; interaction, $F_{(1,23)} = 8.086$, $p = 0.0092$, Bonferroni post hoc analysis, LFS: eGFP mice vs. ChR2 mice, $^{**}p < 0.01$. Open arms entries: two-way ANOVA with repeated measures, main effect of LFS treatment, $F_{(1,23)} = 1.636$, $p = 0.2137$; main effect of virus, $F_{(1,23)} = 1.908$, $p = 0.1805$; interaction, $F_{(1,23)} = 6.283$, $p = 0.0197$, Bonferroni post hoc analysis, LFS: eGFP mice vs. ChR2 mice, $^{*}p < 0.01$. **H** Schematic showing experimental procedures for in vivo high-frequency stimulation (HFS) in control mice that co-injected with oCHIEF-carrying AAV and red Retrobeads. **I** Representative traces showing EPSCs in BLA → dmPFC PNs (left) and summary plots of PPR in BLA → dmPFC PNs (right). Scale bar: 100 ms, 50 pA. Control mice: $n = 8$ neurons/3 mice; HFS mice: $n = 13$ neurons/4 mice. Two-tailed unpaired *t*-test, control vs. HFS, $^{**}p < 0.01$. **J** Representative traces showing EPSCs (left) and Summary plots of PPR in BLA ↛ dmPFC PNs (right). Control mice: $n = 13$ neurons/4 mice; HFS mice: $n = 12$ neurons/4 mice. Two-tailed unpaired *t*-test, control vs. HFS, $^{*}p < 0.05$. **K** Schematic illustration of injection of oCHIEF- or eGFP-carrying AAV in dmPFC. **L** Schematic showing the experimental procedures. **M** representative images showing the injection site in dmPFC (left) and optic fibers placement onto BLA (right). Scale bar: 500 (left) and 100 (right) μm. OFT time in center (**N**) and total distance (**O**) measured HFS. No-HFS: eGFP mice: $n = 6$ mice; 0-CHIEF mice, $n = 7$ mice; HFS: eGFP mice, $n = 7$ mice; oCHIEF mice, $n = 9$ mice. Time in center: two-way ANOVA with repeated measures, main effect of HFS treatment, $F_{(1,25)} = 5.88$, $p = 0.0229$; main effect of virus, $F_{(1,25)} = 2.621$, $p = 0.118$; interaction, $F_{(1,25)} = 2.761$, $p = 0.1091$, Bonferroni post hoc analysis, HFS: eGFP mice vs. oCHIEF mice, $^{*}p < 0.001$. Total distance traveled: two-way ANOVA with repeated measures, main effect of HFS treatment, $F_{(1,25)} = 1.423$, $p = 0.2441$; main effect of virus, $F_{(1,25)} = 0.1473$, $p = 0.7044$; interaction, $F_{(1,25)} = 1.163$, $p = 0.2911$. **P**, **Q** EPM open-arm time (**Q**) and entries (**R**) measured HFS. No-HFS: eGFP mice: $n = 7$ mice; oCHIEF mice, $n = 7$ mice; HFS: eGFP mice, $n = 9$ mice; 0-CHIEF mice, $n = 6$ mice. Time in open arms: two-way ANOVA with repeated measures, main effect of HFS treatment, $F_{(1,25)} = 5.172$, $p = 0.0318$; main effect of virus, $F_{(1,25)} = 7.53$, $p = 0.0111$; interaction, $F_{(1,25)} = 5.674$, $p = 0.0251$, Bonferroni post hoc analysis, HFS: eGFP mice vs. oCHIEF mice, $^{**}p < 0.01$. Open arms entries: two-way ANOVA with repeated measures, main effect of HFS treatment, $F_{(1,25)} = 0.624$, $p = 0.437$; main effect of virus, $F_{(1,25)} = 8.637$, $p = 0.007$; interaction, $F_{(1,25)} = 9.016$, $p = 0.006$, Bonferroni post hoc analysis, HFS: eGFP mice vs. oCHIEF mice, $^{*}p < 0.01$. **R** A working model for acute stress-induced short-term anxiety-like behavior. All data are presented as the mean ± SEM.

we injected AAVs expressing oCHIEF-eGFP into the dmPFC and implanted optical fiber onto the BLA. Four weeks after viral injection, HFS was delivered to the mice, and slices containing BLA were prepared to record the PPR. The results indicated that the HFS protocol robustly decreased the PPR in both neuron populations (Fig. 5H–J). In addition, HFS also increased the mEPSCs frequency which was consistent with the effect of ARS (Supplementary Fig. 10).

After verifying the stimulation protocol, we next investigated whether the high-frequency stimulation of dmPFC fibers in the BLA could increase anxiety-like behavior in naive mice. The experimental procedures are shown in Fig. 5K–M. Compared with eGFP-expressing control mice, oCHIEF-expressing mice spent less time in the center area immediately after HFS treatment (HFS) (Fig. 5N). Notably, the total distance they traveled in OFT was not changed (Fig. 5O), suggesting that the general locomotor activity of mice was not affected. Similarly, the HFS-treated mice also spent less time in and had fewer entries into the open arms during EPMT (Fig. 5P, Q). Taken together, the above findings suggest that enhancing the Pr in dmPFC inputs to the BLA PNs is sufficient to induce anxiety-like behavior in unstressed mice.

DISCUSSION

Our previous studies have demonstrated that chronic stress causes anxiety disorders through input- and output-specific regulation of neuronal plasticity in the BLA [18, 25, 34]. Here, we showed that short-term anxiety-like behavior induced by ARS was associated with increased activity of BLA PNs, which was mainly caused by increased excitatory synaptic transmission, rather than changes in intrinsic neuronal excitability. Specifically, mice subjected to ARS showed input-specific, rather than output-specific, regulation of presynaptic glutamate release at dmPFC-to-BLA synapses (Fig. 5R).

The severity of anxiety largely depends on the intensity, duration, and timing of the stressors. While chronic and severe stress induces long-lasting structural and functional remodeling in the brain and thus may cause anxiety disorders characterized by persistent and excessive anxiety [28, 35–37], acute mild and brief stress can result in short-term anxiety-like behavior that is restricted to a specific time window early following stress exposure. Here, we found that a single 2-h episode of restraint stress increased anxiety-like behavior immediately after stress exposure but could be reversed 24 h later. This finding is consistent with previous studies showing that significantly higher anxiety was found immediately after acute stress in humans and rodents [38, 39]. Similarly, a previous study also showed that acute stress leads to cognitive impairments after 4 h, and these memory impairments are not observed 8 h after the stressor [40]. Notably, a recent study by David et al. showed a significant increase in anxiety-like behavior in mice 24 h following acute stress [41]. These inconsistent results may be due to the use of different stress models. David et al. used inescapable foot-shock stress, a more severe stress paradigms that is commonly used to model posttraumatic stress disorder, while here we used mild restraint stress. Interestingly, Sumantra Chattarji et al. revealed that exposure to acute immobilization stress-induced anxiety-like behavior even 10 days after stress [42–44], although they did not measure the short-term effect on anxiety-like behavior. Considering these different findings, one possible explanation is that we and Sumantra Chattarji's lab used different experimental animal models (C57BL/6J mice vs. Wistar rats) at different developmental stages (adolescent vs. adult). Indeed, our recent findings showed that a single prolonged stress model (2 h restraint, 10 min forced swimming, 15 min predator odor exposure, diethyl ether exposure) has no obvious effect on anxiety-like behavior at 1, 7 or 14 days after stress [45], while this stress model can induce persistent anxiety-like behavior in rats [46].

Considerable evidence has revealed that hyperactivity of the amygdala is strongly associated with the onset and exacerbation of chronic stress-related disorders [18, 25, 36, 47]. For example, our recent studies have indicated that anxiety disorders induced by 10 days of repeated restraint stress increased the activity of BLA PNs through both synaptic (enhancing excitatory transmission) and nonsynaptic (promoting intrinsic neuronal excitability) mechanisms [18, 25, 34], while whether single restraint stress-induced short-term anxiety-like behavior has a uniform or distinct mechanism still remains an open question. Interestingly, in this study, we found that ARS-induced transient activation of BLA

PNs through synaptic (but not nonsynaptic) mechanisms. ARS transiently increased the excitatory (but not inhibitory) synaptic transmission onto BLA neurons, leading to shifts in the balance between excitatory and inhibitory neurotransmission (E/I balance) toward stronger excitation. Considering that the E/I balance is pivotal for proper information processing [17, 43, 48], disturbance of the E/I balance might implicate acute stress-induced short-term anxiety-like behavior. However, we observed that ARS failed to affect the intrinsic excitability of BLA PNs, which is consistent with earlier reports on neural firing after acute stress [35, 49]. It is worth noting that ARS-induced increases in excitatory synaptic transmission onto BLA PNs are normalized 1 day after the stressor, while that induced by chronic stress can persist for a long time after stress [50]. These findings suggest that BLA PNs may become maladaptive when repeatedly exposed to stress, and that loss of this adaptability of BLA PNs may result in psychiatric disorders.

We observed that ARS enhanced excitatory synaptic transmission through presynaptic glutamate release as indicated by a decrease in the PPR. In addition, we found an increased mEPSC frequency. It should be noted that a change in mEPSC frequency indicates an effect on AP-independent spontaneous release of glutamate, whereas PPR correlates with the probability of AP-dependent release. In this case, our findings suggest that both AP-dependent and -independent neurotransmitter release contribute to the ARS-induced increase in presynaptic glutamate release probability. Interestingly, optogenetic weakening of prefrontal glutamate release not only reversed the ARS-induced decrease in PPR but also reduced the frequency of mEPSCs. Although the exact mechanisms are not fully understood, this finding does argue for a critical role of dmPFC input in regulating alterations of ARS-related synaptic transmission onto BLA PNs.

One interesting finding in the current study was that silencing BLA PNs suppressed the frequency of mEPSCs. The mEPSC frequency indicates glutamate release probability from presynaptic terminals, while we here used eNpHR3.0-mCherry which is known to inhibit BLA postsynaptic neurons. Notably, a recent study found that stress exposure induced the excitation of dmPFC neurons, which resulted from the increased neuronal activity of dmPFC projecting BLA neurons. Subsequently, the increased dmPFC neuronal activity in turn enhances synaptic transmission onto BLA PNs. This study raises an interesting positive feedback loop where stress increases glutamate release probability within a reciprocal BLA-dmPFC-BLA circuit [41]. Together with the findings that the BLA neuronal activity and dmPFC-to-BLA synapse were strengthened by ARS, the reduction of the mEPSC frequency following silencing BLA PNs may be achieved through the inhibition of reciprocal BLA-dmPFC-BLA circuit.

The mPFC sends dense projections to the BLA [32] and exhibits "top-down" control of the amygdala. Moreover, the reciprocal mPFC-amygdala circuit has been shown to play a vital role in emotion regulation, memory, and stress response [31, 32, 51]. In this study, we found that ARS increased presynaptic glutamate releases onto BLA PNs from dmPFC afferents, as reflected by the decreased PPR. However, unlike its influence on the dmPFC-BLA pathway, ARS had little influence on presynaptic glutamate release from LA afferents, which is the major input nucleus of the amygdala that relays signals to BLA, suggesting an input-specific regulation of BLA inputs by ARS. Although the exact mechanisms of this specificity remain unknown, one potential explanation is that the LA receives and integrates multiple sensory inputs from cortical and subcortical regions, and electric stimuli activate almost all the fibers around the bipolar electrode placed. Thus, such results may represent the net effect of all activated afferents, which may obscure the true effects of specific pathway activation. Importantly, we established a direct causal link between the increased prefrontal glutamate release onto BLA PNs and the ARS-induced short-term anxiety-like behavior. First, we found that using high-frequency optogenetic stimulation to facilitate the prefrontal glutamate release onto BLA PNs led to increased anxiety-like behavior in unstressed mice. Second, reversing the prefrontal glutamate release in dmPFC-BLA synapses by low-frequency optogenetic stimulation counteracted ARS-induced increases in anxiety-like behavior. These findings highlight an essential role of dysregulated prefrontal cortex-amygdala connectivity in stress-related anxiety.

Another important finding of this study is that there was no output selectivity underlying acute stress-induced anxiety-like behavior since ARS indistinguishably facilitates the synaptic transmission onto BLA neurons projecting to dmPFC (BLA → dmPFC) or elsewhere (BLA ↛ dmPFC) PNs. Such an effect could be adaptatively returned to basal levels 1 day after stress. This is in striking contrast to our recent finding that in a mouse model anxiety disorder, the increased BLA neuronal activity was only observed in BLA ↛ dmPFC PNs but not BLA → dmPFC PNs [18, 25]. However, the exact circuit mechanisms of such specificity remain unknown. We speculate that the adaptations of distinct neuronal populations vary greatly from the other in terms of repeated stress exposure. That is, the BLA → dmPFC PNs may possess a strong adaptive capacity in the face of stress exposure. Notably, since chronic stress consists of days of acute stress, it seems that both BLA → dmPFC PNs and BLA ↛ dmPFC PNs neuronal populations exhibit well adaptation 1 day after a single episode of stress exposure, while the response of BLA ↛ dmPFC PNs becomes maladaptive when they are repeatedly exposed to stress, which results in persistent activation of these neuronal populations and leads to anxiety disorders. Nevertheless, the exact molecular mechanism underlying the (mal-)adaptive capacity of distinct BLA neuronal populations requires future investigation.

In summary, we here demonstrated that acute stress-induced short-term anxiety-like behavior was mediated by increased activity of BLA PNs through synaptic but not nonsynaptic plasticity. These findings, along with our recent reports, might help us better understand the neuronal mechanisms underlying physiological and pathological anxiety in the amygdala. More importantly, the new finding that the stress-induced short-term anxiety-like behavior caused by increased synaptic transmission efficiency from dmPFC input to BLA neurons, while without any effect on intrinsic neuronal excitability, raises the exciting possibility of developing novel therapeutics that target the prefrontal cortex-amygdala connectivity and selectively weaken it, providing a unique therapeutic profile for the treatment of stress-related anxiety disorders.

REFERENCES

1. Raymond JG, Steele JD, Series P. Modeling trait anxiety: from computational processes to personality. Front Psychiatry. 2017;8:1.
2. Shin LM, Liberzon I. The neurocircuitry of fear, stress, and anxiety disorders. Neuropsychopharmacology. 2010;35:169–91.
3. Hariri AR, Holmes A. Finding translation in stress research. Nat Neurosci. 2015;18:1347–52.
4. Katie AM, Laura DK, Erin CD, Robert W, George V, Karestan CK. Childhood social environment, emotional reactivity to stress, and mood and anxiety disorders across the life course. Depress Anxiety. 2010;27:1087–94.
5. MacNeil G, Sela Y, McIntosh J, Zacharko RM. Anxiogenic behavior in the light–dark paradigm following intraventricular administration of cholecystokinin-8S, restraint stress, or uncontrollable footshock in the CD-1 Mouse. Pharmacol Biochem Behav. 1997;58:737–46.
6. McEwen BS. Brain on stress: how the social environment gets under the skin. Proc Natl Acad Sci USA 2012;109:17180–5.
7. Arnsten FT. Stress weakens prefrontal networks: molecular insults to higher cognition. Nat Neurosci. 2015;18:1376–85.
8. Jovanovic T, Ressler KJ. How the neurocircuitry and genetics of fear inhibition may inform our understanding of PTSD. Am J Psychiat. 2010;167:648–62.
9. Di S, Itoga CA, Fisher MO, Solomonow J, Roltsch EA, Gilpin NW, et al. Acute stress suppresses synaptic inhibition and increases anxiety via endocannabinoid release in the basolateral amygdala. J Neurosci. 2016;36:8461–70.
10. Zhang WH, Zhang JY, Holmes A, Pan BX. Amygdala circuit substrates for stress adaptation and adversity. Biol Psychiatry. 2021;89:847–56.

11. Roozendaal B, McEwen BS, Chattarji S. Stress, memory and the amygdala. Nat Rev Neurosci. 2009;10:423–33.
12. Kalin NH, Shelton SE, Davidson RJ. The role of the central nucleus of the amygdala in mediating fear and anxiety in the primate. J Neurosci. 2004;24:5506–15.
13. Tripathi SJ, Chakraborty S, Rao BSS. Remediation of chronic immobilization stress-induced negative affective behaviors and altered metabolism of monoamines in the prefrontal cortex by inactivation of basolateral amygdala. Neurochem Int. 2020;141:104858.
14. Beyeler A, Namburi P, Glober GF, Simonnet C, Calhoon GG, Conyers GF, et al. Divergent routing of positive and negative information from the amygdala during memory retrieval. Neuron. 2016;90:348–61.
15. Felix-Ortiz AC, Burgos-Robles A, Bhagat ND, Leppla CA, Tye KM. Bidirectional modulation of anxiety-related and social behaviors by amygdala projections to the medial prefrontal cortex. Neuroscience. 2016;321:197–209.
16. Felix-Ortiz AC, Beyeler A, Seo C, Leppla CA, Wildes CP, Tye KM. BLA to vHPC inputs modulate anxiety-related behaviors. Neuron. 2013;79:658–64.
17. Liu WZ, Zhang WH, Zheng ZH, Zou JX, Liu XX, Huang SH, et al. Identification of a prefrontal cortex-to-amygdala pathway for chronic stress-induced anxiety. Nat Commun. 2020;11:2221.
18. Zhang WH, Liu WZ, He Y, You WJ, Zhang JY, Xu H, et al. Chronic stress causes projection-specific adaptation of amygdala neurons via small-conductance calcium-activated potassium channel downregulation. Biol Psychiatry. 2019;85:812–28.
19. Pribiag H, Shin S, Wang EH, Sun F, Datta P, Okamoto A, et al. Ventral pallidum DRD3 potentiates a pallido-habenular circuit driving accumbal dopamine release and cocaine seeking. Neuron. 2021;109:2165–82.
20. Huang SH, Liu WZ, Qin X, Guo CY, Xiong QC, Wang Y, et al. Association of increased amygdala activity with stress-induced anxiety but not social avoidance behavior in mice. Neurosci Bull. 2022;38:16–28.
21. Pan HQ, Zhang WH, Liao CZ, He Y, Xiao ZM, Qin X, et al. Chronic stress oppositely regulates tonic inhibition in thy1-expressing and non-expressing neurons in amygdala. Front Neurosci. 2020;14:299–313.
22. Fang X, Jiang S, Wang J, Bai Y, Kim CS, Blake D, et al. Chronic unpredictable stress induces depression-related behaviors by suppressing AgRP neuron activity. Mol Psychiatry. 2021;26:2299–316.
23. Cynthia MC, Rosenkranz JA, Anthony AG. Chronic cold stress alters prefrontal cortical modulation of amygdala neuronal activity in rats. Biol Psychiatry. 2005;58:382–91.
24. Tan T, Wang W, Liu T, Zhong P, Conrow-Graham M, Tian X, et al. Neural circuits and activity dynamics underlying sex-specific effects of chronic social isolation stress. Cell Rep. 2021;34:108874–91.
25. Zhang JY, Liu TH, He Y, Pan HQ, Zhang WH, Yin XP, et al. Chronic stress remodels synapses in an amygdala circuit-specific manner. Biol Psychiatry. 2019;85:189–201.
26. O'Leary TP, Sullivan KE, Wang L, Clements J, Lemire AL, Cembrowski MS. Extensive and spatially variable within-cell-type heterogeneity across the basolateral amygdala. Elife. 2020;9:59003–30.
27. Tovote P, Fadok JP, Luthi A. Neuronal circuits for fear and anxiety. Nat Rev Neurosc. 2015;16:317–31.
28. Bittar TP, Pelaez MC, Hernandez Silva JC, Quessy F, Lavigne AA, Morency D, et al. Chronic stress induces sex-specific functional and morphological alterations in corticoaccumbal and corticotegmental pathways. Biol Psychiatry. 2021;90:194–205.
29. Robinson OJ, Krimsky M, Lieberman L, Phillip A, Katherine V, Grillon C. The dorsal medial prefrontal (anterior cingulate) cortex–amygdala aversive amplification circuit in unmedicated generalised and social anxiety disorders: an observational study. Lancet Psychiatry. 2014;1:294–302.
30. McGarry LM, Carter AG. Prefrontal cortex drives distinct projection neurons in the basolateral amygdala. Cell Rep. 2017;21:1426–33.
31. McGinnis MM, Parrish BC, Chappell AM, Alexander NJ, McCool BA. Chronic ethanol differentially modulates glutamate release from dorsal and ventral prefrontal cortical inputs onto rat basolateral amygdala principal neurons. eNeuro. 2020;7:0132–19. https://doi.org/10.1523/ENEURO.0132-19.2019.
32. Cho JH, Deisseroth K, Bolshakov VY. Synaptic encoding of fear extinction in mPFC-amygdala circuits. Neuron. 2013;80:1491–507.
33. Zhou TT, Zhu H, Fan ZX, Wang F, Chen Y, Liang HX, et al. History of winning remodels thalamo-PFC circuit toreinforce social dominance. Science. 2017;357:162–8.
34. Qin X, He Y, Wang N, Zou JX, Zhang YM, Cao JL, et al. Moderate maternal separation mitigates the altered synaptic transmission and neuronal activation in amygdala by chronic stress in adult mice. Mol Brain. 2019;12:111–23.
35. Rosenkranz JA, Venheim ER, Padival M. Chronic stress causes amygdala hyperexcitability in rodents. Biol Psychiatry. 2010;67:1128–36.
36. Rau AR, Chappell AM, Butler TR, Ariwodola OJ, Weiner JL. Increased basolateral amygdala pyramidal cell excitability may contribute to the anxiogenic phenotype induced by chronic early-life stress. J Neurosci. 2015;35:9730–40.
37. Yun SH, Reynolds RP, Petrof I, White A, Rivera PD, Segev A, et al. Stimulation of entorhinal cortex–dentate gyrus circuitry is antidepressive. Nat Med. 2018;24:658–66.
38. Solomonow J, Tasker JG. Anxiety behavior induced in mice by acute stress. Tula Undergrad Res J. 2015;2:14–9.
39. Robinson SJ, Sunram-Lea SI, Leach J, Owen-Lynch PJ. The effects of exposure to an acute naturalistic stressor on working memory, state anxiety and salivary cortisol concentrations. Stress. 2008;11:115–24.
40. Jene T, Gassen NC, Opitz V, Endres K, Muller MB, van der Kooij MA. Temporal profiling of an acute stress-induced behavioral phenotype in mice and role of hippocampal DRR1. Psychoneuroendocrinology. 2018;91:149–58.
41. Marcus DJ, Bedse G, Gaulden AD, Ryan JD, Kondev V, Winters ND, et al. Endocannabinoid signaling collapse mediates stress-induced amygdalo-cortical strengthening. Neuron. 2020;105:1062–76.
42. Mitra R, Jadhav S, McEwen BS, Vyas A, Chattarji S. Stress duration modulates the spatiotemporal patterns of spine formation in the basolateral amygdala. Proc Natl Acad Sci USA 2005;102:9371–6.
43. Gupta K, Chattarji S. Sex differences in the delayed impact of acute stress on the amygdala. Neurobiol Stress. 2021;14:100292.
44. Chakraborty P, Chattarji S. Interventions after acute stress prevent its delayed effects on the amygdala. Neurobiol Stress. 2019;10:100168.
45. You WJ, He Y, Liu WZ, Zhu YG, Hu P, Pan BX, et al. Exposure to single prolonged stress fails to induce anxiety-like behavior in mice. Stress Brain. 2021;1:145.
46. Han F, Ding JL, Shi YX. Expression of amygdala mineralocorticoid receptor and glucocorticoid receptor in the single-prolonged stress rats. BMC Neurosci. 2014;15:77–88.
47. Zheng ZH, Tu JL, Li XH, Hua Q, Liu WZ, Liu Y, et al. Neuroinflammation induces anxiety- and depressive-like behavior by modulating neuronal plasticity in the basolateral amygdala. Brain Behav Immun. 2021;91:505–18.
48. Yu W, Wang L, Yang L, Li YJ, Wang M, Qiu C, et al. Activation of LXRbeta signaling in the amygdala confers anxiolytic effects through rebalancing excitatory and inhibitory neurotransmission upon acute stress. Neurotherapeutics. 2020;17:1253–70.
49. Song C, Zhang WH, Wang XH, Zhang JY, Tian XL, Yin XP, et al. Acute stress enhances the glutamatergic transmission onto basoamygdala neurons embedded in distinct microcircuits. Mol Brain. 2017;10:3–13.
50. Qin X, Liu XX, Wang Y, Wang D, Song Y, Zou JX, et al. Early life stress induces anxiety-like behavior during adulthood through dysregulation of neuronal plasticity in the basolateral amygdala. Life Sci. 2021;285:119959–68.
51. Kim MJ, Whalen PJ. The structural integrity of an amygdala-prefrontal pathway predicts trait anxiety. J Neurosci. 2009;29:11614–8.

AUTHOR CONTRIBUTIONS

WZ, WL, and BP conceived the study. WL, SH, YW, CW, HP, and KZ performed the experiments. WL, YW, and PH analyzed the data. WZ and WL wrote the manuscript.

FUNDING

This work was supported by grants from National Natural Science Foundation of China (Grant Nos. 81930032 and 82125010 to BP, 32222034 and 31970953 to WZ, 82101589 to WL, 32160193 to HP), National Key R&D Program of China (2021ZD0202704 to BP), Natural Science Foundation of Jiangxi Province (20212ACB206038 to WZ, 20192ACB20023 to BP), and China Postdoctoral Science Foundation (Grant Nos. 2021TQ0138 and 2021M701545 to WL). Interdisciplinary Innovation Fund of Natural Science, Nanchang University (9167-27060003-ZD2102 to WZ).

COMPETING INTERESTS

The authors declare no competing interests.

ADDITIONAL INFORMATION

Supplementary information The online version contains supplementary material available at https://doi.org/10.1038/s41386-022-01515-x.

Correspondence and requests for materials should be addressed to Bing-Xing Pan or Wen-Hua Zhang.